The two-dimensional electron gas of the In_2O_3 surface: Enhanced thermopower, electrical transport properties, and its reduction by adsorbates or compensating acceptor doping

Alexandra Papadogianni,[1] Julius Rombach,[1] Theresa Berthold,[2] Vladimir Polyakov,[3] Stefan Krischok,[2] Marcel Himmerlich,[2,4] and Oliver Bierwagen[1]

[1]*Paul-Drude-Institut für Festkörperelektronik, Leibniz-Institut im Forschungsverbund Berlin e.V., Hausvogteiplatz 5–7, D–10117 Berlin, Germany*
[2]*Institut für Physik und Institut für Mikro- und Nanotechnologien, Technische Universität Ilmenau, PF 100565, D–98684 Ilmenau, Germany*
[3]*Fraunhofer-Institut für Angewandte Festkörperphysik, Tullastraße 72, D-79108 Freiburg, Germany*
[4]*CERN, European Organization for Nuclear Research, 1211 Meyrin, Switzerland*

(Dated: March 11, 2020)

arXiv:2003.04631v1 [physics.app-ph] 10 Mar 2020

In_2O_3 is an n-type transparent semiconducting oxide possessing a surface electron accumulation layer (SEAL) like several other relevant semiconductors, such as InAs, InN, SnO_2, and ZnO. Even though the SEAL is within the core of the application of In_2O_3 in conductometric gas sensors, a consistent set of transport properties of this two-dimensional electron gas (2DEG) is missing in the present literature. To this end, we investigate high quality single-crystalline as well as textured doped and undoped In_2O_3(111) films grown by plasma-assisted molecular beam epitaxy (PA-MBE) to extract transport properties of the SEAL by means of Hall effect measurements at room temperature while controlling the oxygen adsorbate coverage via illumination. The resulting sheet electron concentration and mobility of the SEAL are $\approx 1.5 \times 10^{13}$ cm^{-2} and ≈ 150 cm^2/Vs, respectively, both of which get strongly reduced by oxygen-related surface adsorbates from the ambient air. Our transport measurements further demonstrate a systematic reduction of the SEAL by doping In_2O_3 with the deep compensating bulk acceptors Ni or Mg. This finding is supported by X-ray photoelectron spectroscopy (XPS) measurements of the surface band bending and SEAL electron emission. Quantitative analyses of these XPS results using self-consistent, coupled Schrödinger–Poisson calculations indicate the simultaneous formation of compensating bulk donor defects (likely oxygen vacancies) which almost completely compensate the bulk acceptors. Finally, an enhancement of the thermopower by reduced dimensionality is demonstrated in In_2O_3: Seebeck coefficient measurements of the surface 2DEG with partially reduced sheet electron concentrations between 3×10^{12} and 7×10^{12} cm^{-2} (corresponding average volume electron concentration between 1×10^{19} and 2.3×10^{19} cm^{-3}) indicate a value enhanced by $\approx 80\,\%$ compared to that of bulk Sn-doped In_2O_3 with comparable volume electron concentration.

I. INTRODUCTION

Indium oxide (In_2O_3) is a transparent semiconducting oxide, which exhibits inherent n-type conductivity, commonly referred to as unintentional doping (UID). Like the related or SnO_2[1], In_2O_3 possesses a surface electron accumulation layer (SEAL)[2], that lies within the core of In_2O_3-based conductometric gas sensors for oxygen species.[3] Along with this, In_2O_3 typically finds applications as a transparent contact in optoelectronic devices, mostly in its highly Sn-doped form, known as ITO[4–6], which can reach electron concentrations as high as $10^{21}\,$cm^{-3}. This particular application of In_2O_3 further benefits from the existence of the SEAL, which favors the formation of Ohmic contacts. This property, nevertheless, indicates that the formation of Schottky contacts—required for several other applications—is hindered by the existence of the SEAL, even for high work function metals like Pt[7,8]. Tunability of the SEAL is, hence, necessary to both unlock the entire spectrum of potential device applications of In_2O_3 and tune its gas sensitivity.

Using X-ray photoelectron spectroscopy (XPS) measurements King *et al.*[9] demonstrated the existence of a few-nm thick electron accumulation layer at the surface of In_2O_3 by a downward band bending at the surface of undoped single-crystalline films, in contradiction to previous investigations reporting a surface depletion.[10,11] This discrepancy mainly arose due the difference in the assumed fundamental band gap of In_2O_3 required for the interpretation of the XPS results: While the optical bandgap of ≈3.7 eV has been assumed to equal the fundamental one by the authors of Ref. 10 and 11, the authors of Ref. 9 have assumed a dipole-forbidden, fundamental band gap of ≈ 2.6 eV — in agreement with state-of-the art *ab-initio* theory combined with bulk and surface sensitive XPS measurements.[12] A general explanation for the existence of the In_2O_3 SEAL has been given within the context of the charge neutrality level (CNL), also known as branch point energy. Defect states at the CNL acquire their weight equally from the valence and conduction bands,[13] essentially rendering the CNL a demarcation between donor- and acceptorlike defect states. In contrast to most other semiconductors, in the case of In_2O_3 the CNL lies within the conduction band,[9,14] due to its particular bulk band structure, with a very

prominent, low lying conduction band minimum (CBM) at the Γ-point and an almost flat valence band. Donorlike states at the surface of In_2O_3 pin the surface Fermi level, E_F, slightly below the CNL, causing a downward bending of the conduction and valence bands. Breaking of the translational symmetry of the bulk can give rise to such donorlike surface states.[15] Besides that, for films exposed to the ambient, the enhanced conductivity of the surface has also been attributed to adsorbates attaching to it; an effect not observed for films that have undergone *in situ* cleavage of the surface.[16] The microscopic origin of the SEAL, has been further associated with surface oxygen vacancies acting as doubly ionized shallow donors V_O^{2+}[17] and their strongly reduced defect formation energy.[18] Finally, surface In adatoms, which are energetically favored over V_O,[19] can also act as shallow donors[20] and have been experimentally demonstrated on the $In_2O_3(111)$ surface after a reducing surface preparation [annealing at 300–500 °C in ultra-high vacuum (UHV)].[19]

For 111-oriented films grown by plasma-assisted molecular beam epitaxy (PA-MBE), like the ones studied in the current work, the surface electron concentration has been shown to have a peak value at $8 \times 10^{19}\,\mathrm{cm}^{-3}$[2], similar to the results from Schrödinger–Poisson modeling on the SEAL of melt-grown bulk In_2O_3 single crystal studied in Ref. 21. Moreover, angle-resolved photoelectron spectroscopy (ARPES) measurements have confirmed the two-dimensional electron gas (2DEG) nature of the SEAL with sheet electron concentration of $4 \times 10^{13}\,\mathrm{cm}^{-2}$ after surface preparation at high temperature (by repeated cycles of Ar^+ sputtering (500 eV) and annealing at 600 °C in UHV for 1 h)[17] and $2 \times 10^{13}\,\mathrm{cm}^{-2}$ after surface preparation at intermediate temperature (annealing at 300 °C in UHV for ≈ 15 min).[22] Both of the surface preparations employed within those studies are prone to reduce the surface—that is increase the concentration of surface V_O or In adatoms acting as surface donors and, thus, result in a stronger SEAL (i.e. with a higher electron concentration) compared to that of an unprepared sample.

Significant reduction of a SEAL by compensating bulk acceptors has been previously demonstrated in InN by Mg acceptor doping.[23] Previous studies[24,25] have shown that acceptors like Ni and Mg have a compensating effect on the bulk electron transport of In_2O_3. This effect, however, is revealed after an additional annealing of the material in oxygen, which has been explained by overcompensation of the added acceptors due to the simultaneous formation of donorlike point defects—most likely V_O—during growth:[24,25] The addition of acceptor elements lowers the Fermi energy and, according to Refs. 26 and 27, this reduces the formation energy of V_O—thus promoting their incorporation into the crystal lattice. Studies regarding the position of the bulk donor levels in the band gap associated with oxygen vacancies have been rather inconclusive, with some works indicating V_O to have deep donor levels[26,27] and others to potentially be shallow donors[28–30]. Whether the annealing completely removed the doping-induced V_O could not be clarified in Refs. 24 and 25. Fig. 1 (a) shows schematically the effect of bulk acceptor doping on the position of the E_F and the band alignment, with emphasis on its impact on the SEAL, assuming neither spontaneous formation of compensating donors nor their removal with a treatment such as oxygen annealing. For comparison, Fig. 1 (b) shows the position of the E_F and band alignment in a UID In_2O_3.

Early studies on the conductivity of In_2O_3 at elevated temperatures have already documented its dependence on the oxygen content of the sample environment[31], which is the basis of its application as the active material in conductometric gas sensors. At sufficiently low temperatures, that preclude oxygen diffusion in the lattice, this sensing behavior is related to the surface-acceptor role of adsorbed oxygen species that can reduce the SEAL by electron transfer.[32,33] The effect of acceptorlike air adsorbates on the band banding and, hence, occupation of the SEAL is schematically shown in Fig. 1 (c). Such gas sensors are typically (re)activated by heating the sensing material at elevated temperatures (typically a few hundred ° C). Efforts towards a more energy-efficient solution have demonstrated In_2O_3 gas-sensors operating at room temperature reactivated by ultraviolet (UV) light induced photoreduction[34–36]. During photoreduction the illumination forces the desorption of the negatively charged oxygen adsorbates[37] through recombination with the photogenerated holes while the photogenerated electrons remain in the In_2O_3.[38] The SEAL sheet conductivity of PA-MBE grown In_2O_3 films in air has been reported to be 3×10^{-4} S in the photoreduced stationary state (under UV illumination)[3] and below 2.2×10^{-5} S with oxygen adsorbates (i.e., without illumination).[39] A reduction of the SEAL in those films by oxygen adsorbates has been independently demonstrated by conductance and XPS measurements.[3,33] However, these earlier works do not provide any information concerning the actual electron concentration at the In_2O_3 surface.

There have, thus, been no reports regarding the full set of the SEAL transport properties (sheet conductivity and sheet electron concentration) measured with a single technique, after a defined surface treatment, and in a defined environment—as has long been accomplished for ZnO[40], for instance. Furthermore, there is no information in the literature concerning the thermoelectric properties of the SEAL. In addition to the strong interest in discovering and understanding the thermoelectric transport properties and mechanisms of such 2DEGs, knowledge of the SEAL properties is necessary for the application aspect of the material, as it enables controllable fine-tuning of the (thermo)electrical behavior of the In_2O_3 surface.

The current work consistently determines the surface transport properties of In_2O_3 and demonstrates the intentional and controllable reduction of the sheet electron concentration at the surface of In_2O_3 by incorporation of the compensating bulk acceptors Ni and Mg or by oxygen

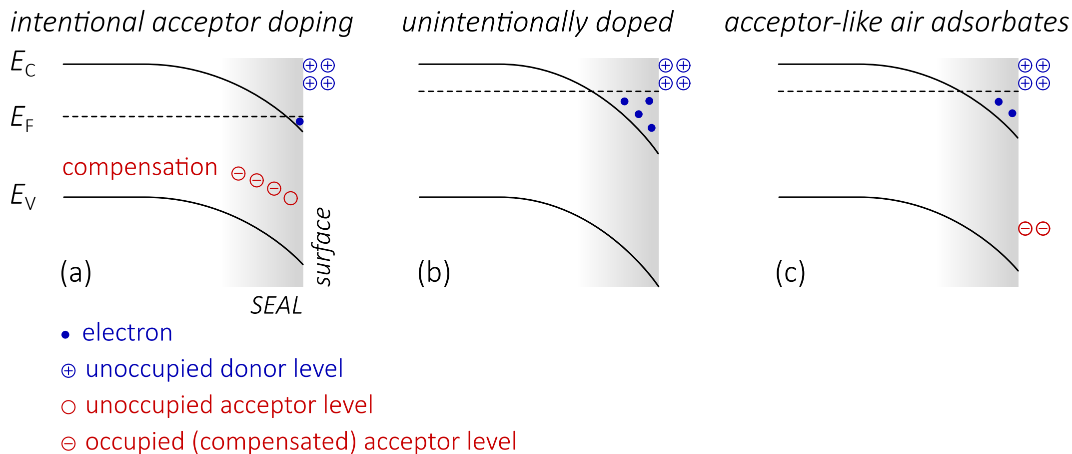

Figure 1. Schematic representation of the band alignment for (a) intentional doping with bulk acceptors and the corresponding compensation of the SEAL, (b) unintentionally doped In_2O_3, and (c) unintentional compensation of the SEAL due to adsorption of acceptorlike oxidizing species. The difference $(N^+_{D,S} - N^-_{A,S})$ of the 2D concentration of charged surface donors and acceptors provides a net surface charge N_{SS}.

surface adsorbates. This is accomplished with the combination of Hall effect transport measurements (with and without UV illumination) and X-ray photoelectron spectroscopy. Supporting self-consistent Schrödinger–Poisson calculations reveal a close compensation of the bulk acceptors by oxygen vacancies even after annealing the samples in oxygen. Finally, the thermoelectric properties of the surface electron accumulation layer are investigated by Seebeck coefficient measurements. As previously demonstrated for ZnO[41], the 2DEG at the In_2O_3 surface is shown to also exhibit an increased thermopower in comparison bulk Sn-doped films with comparable volume electron concentration.

II. EXPERIMENT

For the purposes of this study, high quality (111)-oriented In_2O_3 has been synthesized by PA-MBE. Single-crystalline UID and Ni-doped films have been grown on quarters of 2” insulating ZrO_2:Y (YSZ) (111) substrates, whereas full 2” Al_2O_3 (0001) (c-plane Al_2O_3) substrates have been employed for the growth of UID and Mg-doped textured films. After growth, all samples have been further cleaved into smaller pieces with a size of approximately $5 \times 5\,\mathrm{mm}^2$. The total thickness of the films ranges between 350–500 nm. Further details on the growth of the studied samples are reported in Ref. 24 (single-crystalline) and Ref. 3 (textured).

In order to largely remove compensating donors, all samples under study have been annealed in oxygen within a rapid thermal annealing (RTA) system at 800 °C at atmospheric pressure for 60 s. The undoped samples have also been annealed in oxygen to serve as references with comparable characteristics.

For reference measurements, an oxygen plasma treatment of the surface at room temperature was performed in a 13.56 MHz inductively coupled plasma (ICP) reactive ion-etching (RIE) system (Samco Inc., RIE-400iP; process pressure, 0.025 mbar; oxygen flow, 10 standard cubic centimeters per minute; ICP power, 100 W; RIE power, 50 W; treatment time, 5 min) in order to completely deplete surface-near electrons, resulting in an upward surface band bending and complete removal the surface conductivity.[39,42] During this treatment, a high density of reactive oxygen species attach to the In_2O_3 surface, removing electrons from the In_2O_3 to form negatively charged adsorbates.[42] We found this adsorbate layer to be stable against UV-illumination and to be removable only by annealing the material.

The electrical sheet conductivity of the films under study is determined by sheet resistance measurements in the commonly used van der Pauw (vdP) arrangement. In combination with Hall effect measurements, which directly provide the sheet electron concentration, this helps identify the Hall electron mobility of the samples.

Since the measurements throughout this work are performed in ambient environment, oxygen species from the air are expected to adsorb and alter the transport properties of the SEAL. To circumvent this effect, the samples under study have been exposed to UV illumination to force desorption of those species. A light emitting diode (LED) that can generate up to 12 mW ultraviolet (UV) A radiation with a wavelength of 400 nm is utilized for this purpose. The corresponding photon energy of 3.1 eV is above the fundamental, dipole forbidden bandgap and below the onset of strong optical absorption.[12] The associated penetration depth in In_2O_3 is ≈1 µm,[43] i.e., larger than the thickness of the investigated films. For most measurements the LED is operated at a current of 13 mA, which corresponds to approximately 8 mW of optical power, and the illuminated area nominally covers the entire sample surface. This corresponds to a photon flux of approximately $6 \times 10^{20}\,\mathrm{m}^{-2}\mathrm{s}^{-1}$. Due to the UV-induced

desorption of species the conductivity of the surface—and thus the total conductivity of the film—increases with time until it starts saturating once a desorption–adsorption equilibrium has been reached. Representative desorption/adsorption cycles due to UV on/UV off periods can be found in Ref. 3. For the measurements to be reproducible, all samples are exposed to UV for approximately 10 minutes, which has been found sufficient to obtain desorption-adsorption equilibrium.

For the X-ray Photoelectron Spectroscopy (XPS) measurements, the samples were mounted onto Ta sample holders, with the In_2O_3 layer electrically grounded, and inserted into an ultra-high vacuum (UHV) system for surface analysis. The measurements were performed—after preparation of the surface with UV illumination in vacuum at room temperature—in normal emission using monochromated AlKα ($h\nu = 1486.7\,\text{eV}$) radiation and a hemispherical electron analyzer. More details about the setup and the experimental conditions used for this study can be found in Ref. 44. The binding energy scale and the position of the Fermi level are regularly calibrated for clean metal reference samples and the data analysis was performed in analogy to the studies of UID and Mg-doped In_2O_3 films in Ref. 42. The region around the E_F was measured with an extended integration time.

Finally, the acquisition of the thermopower, otherwise known as Seebeck coefficient, was performed as described in detail for In_2O_3 in Ref. 45. The Seebeck coefficient of the SEAL has been calculated by the multilayer method described in Refs. 46 and 47 and then matched to the corresponding 2D electron concentrations—determined by the Hall effect—for measurements with the same sheet resistance (adjusted by proper UV illumination) using the van der Pauw method. This is done because the Seebeck and Hall effect measurements are performed in two separate systems and the sheet resistance is the only property that can be measured in both setups and ensure same surface conditions.

III. RESULTS AND DISCUSSION

A. Transport properties of the adsorbate-attenuated and unattenuated SEAL extracted by the multilayer method

In order to extract the transport properties of the surface carrier system of In_2O_3 the multilayer method described in Refs. 46 and 47 will be employed. Essentially, since all transport systems in our films (depicted in Fig. 2(a)) are connected in parallel, the total sheet conductivity of the film will be the sum of the separate sheet conductivities of the carrier systems comprising it

$$G_\mathrm{tot} = G_\mathrm{B} + G_\mathrm{I} + G_\mathrm{S} \tag{1}$$

where the subscripts indicate the *bulk* (B), *interface* (I), and *surface* (S) sheet conductivity. Let us assume the case depicted in Fig. 2 with two films, (a) and (b), comprising of the same carrier systems—bulk and interface—with the exception of the SEAL, which is not present in film (b). Based on the model described, the sheet conductivity of the carrier system these films differ by, (c), could be extracted by subtracting the total sheet conductivities of the two films. A technique to deplete the SEAL is thus required for this method to be applied.

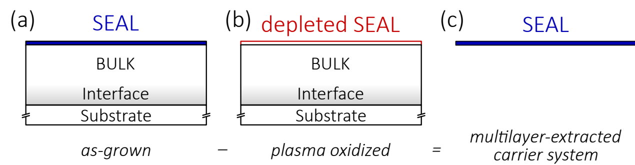

Figure 2. Schematic representation of the carrier systems in the films under study. The substrate is insulating, while it has been shown that the samples under study possess a strong interface carrier system along with the bulk of the film and the SEAL[24]. (a) All carrier systems included in the as-grown film, (b) depleted SEAL in the plasma oxidized film, (c) extracted SEAL by the multilayer method of Refs. 46 and 47.

The plasma oxidation of the surface described in the experimental part can provide samples with depleted SEAL. This indicates that the sheet conductivity of a plasma oxidized sample equals $G_\mathrm{PLOX} = G_\mathrm{B} + G_\mathrm{I}$. Combining this with the multilayer model of Refs. 46 and 47 allows one to extract not only the sheet conductivity, but also the entire set of transport properties of the SEAL by performing Hall effect measurements on an unintentionally doped (UID) sample of In_2O_3 before and after plasma treatment. As an example, one can extract the sheet conductivity of the SEAL as

$$G_\mathrm{S}^\mathrm{w/\,ads.} = G_\mathrm{a.g.} - G_\mathrm{PLOX} \tag{2}$$

where a.g. is used to denote the untreated (besides oxygen annealing), as-grown state of the film. This of course would correspond to an upper estimate of the sheet conductivity of the SEAL with the effect of present air adsorbates (superscript “w/ ads.”). In our UID, single crystalline film we found such a SEAL to feature a sheet conductivity of $G_\mathrm{S} = 3.80 \times 10^{-6}\,\mathrm{S}$, which is significantly lower than that of the photoreduced SEAL ($G \approx 3 \times 10^{-4}\,\mathrm{S}$) in Ref. 3 and suggests that the oxygen adsorbates from the air almost completely deplete the SEAL.

Since the plasma oxidation of the surface could potentially deplete part of the bulk, the extracted sheet conductivity from Eq. 2 could contain the near surface bulk conductivity that got depleted. In order to avoid these effects being reflected on the extracted SEAL transport properties, one can extract the sheet conductivity of the adsorbate-free (superscript “w/o ads.”) SEAL as follows

$$G_\mathrm{S}^\mathrm{w/o\,ads.} = \left(G_\mathrm{a.g.}^\mathrm{UV} - G_\mathrm{a.g.}^\mathrm{dark}\right) - \left(G_\mathrm{PLOX.}^\mathrm{UV} - G_\mathrm{PLOX}^\mathrm{dark}\right) \tag{3}$$

assuming the UV light exposure to remove all surface adsorbates by photoreduction and full depletion of the

SEAL in the dark by adsorbed oxygen species. At this point, it should be pointed out that the high penetration depth of the UV illumination could induce photoconduction in the bulk of the material. Examination of the conductivity change upon UV illumination of an undoped In_2O_3 film, whose surface had been depleted by undergoing the plasma oxidation process, showed a sudden drop of the sheet conductivity by 2.82×10^{-5} S, which amounts up to 7% of the total change in sheet conductivity by the UV as observed in the untreated sample. This bulk photoconduction effect is also excluded by the difference method of Eq. 3.

The method described in Refs. 46 and 47 allows for the extraction of the full set of SEAL transport properties. According to these, the mobility and Seebeck coefficient can both be extracted in a similar manner using respectively

$$\mu_{\mathrm{S}}^{\mathrm{w/o\,ads.}} = \frac{\mu_{\mathrm{a.g.}}^{\mathrm{UV}} \cdot G_{\mathrm{a.g.}}^{\mathrm{UV}} - \mu_{\mathrm{a.g.}}^{\mathrm{dark}} \cdot G_{\mathrm{a.g.}}^{\mathrm{dark}}}{G_{\mathrm{S}}^{\mathrm{w/o\,ads.}}} - \frac{\mu_{\mathrm{PLOX}}^{\mathrm{UV}} \cdot G_{\mathrm{PLOX.}}^{\mathrm{UV}} - \mu_{\mathrm{PLOX}}^{\mathrm{dark}} \cdot G_{\mathrm{PLOX}}^{\mathrm{dark}}}{G_{\mathrm{S}}^{\mathrm{w/o\,ads.}}} \tag{4}$$

$$S_{\mathrm{S}}^{\mathrm{w/o\,ads.}} = \frac{S_{\mathrm{a.g.}}^{\mathrm{UV}} \cdot G_{\mathrm{a.g.}}^{\mathrm{UV}} - S_{\mathrm{a.g.}}^{\mathrm{dark}} \cdot G_{\mathrm{a.g.}}^{\mathrm{dark}}}{G_{\mathrm{S}}^{\mathrm{w/o\,ads.}}} - \frac{S_{\mathrm{PLOX}}^{\mathrm{UV}} \cdot G_{\mathrm{PLOX.}}^{\mathrm{UV}} - S_{\mathrm{PLOX}}^{\mathrm{dark}} \cdot G_{\mathrm{PLOX}}^{\mathrm{dark}}}{G_{\mathrm{S}}^{\mathrm{w/o\,ads.}}} \tag{5}$$

Finally, the sheet (2D) electron concentration of the SEAL without the effect of air adsorbates can be easily calculated based on the results of Eqs. 3 and 4 as

$$n_{\mathrm{S}}^{w/o\,ads} = \frac{G_{\mathrm{S}}^{\mathrm{w/o\,ads.}}}{q\mu_{\mathrm{n}}^{\mathrm{w/o\,ads.}}} \tag{6}$$

where q is the elementary charge. Based on the equations above, the SEAL of an undoped single-crystalline In_2O_3 film has been found to exhibit a sheet conductivity of $G_{\mathrm{S}}^{\mathrm{w/o\,ads.}} = 3.26 \times 10^{-4}$ S, a sheet electron concentration of $n_{\mathrm{S}}^{\mathrm{w/o\,ads.}} = 1.45 \times 10^{13}\,\mathrm{cm}^{-2}$, and a Hall electron mobility of $\mu_{\mathrm{S}}^{w/o\,ads} = 155\,\mathrm{cm^2V^{-1}s^{-1}}$ without the effect of air adsorbates.

B. Intentional attenuation by compensating acceptor doping

Electrical transport

Figure 3 depicts the SEAL transport properties extracted from the Hall measurements by Eqs. (3, 4, and 6) of a series of single-crystalline Ni-doped (blue circles) and textured Mg-doped (red stars) films, along with their dedicated unintentionally doped samples. Increasing compensating doping leads—as expected—to a decrease in the extracted sheet conductivity of the SEAL for both types of dopants and substrates. A Ni concentration of approximately $2 \times 10^{19}\,\mathrm{cm}^{-3}$—which is comparable to the peak surface electron concentration of Ref. 2—has a significant effect on it, whereas a similar concentration of Mg, $N_{\mathrm{Mg}} = 10^{19}\,\mathrm{cm}^{-3}$ does not substantially affect the SEAL transport properties. Higher Ni-doping $> 10^{20}\,\mathrm{cm}^{-3}$ seems to deplete most of the surface carriers, reaching SEAL sheet conductivities as low as 10^{-6} S and a very low Hall mobility, that does not allow for the extraction of a meaningful surface electron concentration. Interestingly, an even higher Mg concentration of $N_{\mathrm{Mg}} = 5\times10^{20}\,\mathrm{cm}^{-3}$ does not fully deplete the SEAL. Besides the doping ranges presented in Fig. 3, a higher Ni doped sample on YSZ (111) with $N_{\mathrm{Ni}} = 2\times10^{21}\,\mathrm{cm}^{-3}$ has been also studied and shown (in Ref. 24) to be insulating, in which case all carrier systems—including the SEAL—have been fully depleted.

To compare with the degree of depletion attained unintentionally by air adsorbates, the data in Fig. 3 represented by full circles demonstrate the sheet conductivity of one UID and one lightly Ni-doped sample that have been measured under dark conditions. The effect of air adsorbates with an acceptorlike behavior is evidently intense, as they decrease the sheet conductivity of the films by two orders of magnitude.

Both the sheet electron concentration and mobility of the SEAL decrease with increasing acceptor concentration, as would have been anticipated for compensating dopants and the addition of charged scattering centers.

However, there seems to be a different doping threshold between the two sample series, which results in stronger or full depletion of the SEAL, and they exhibit different mobilities. In particular, the SEAL mobility of the single crystalline Ni-doped films is significantly lower than the mobility of the Mg-doped ones on c-Al_2O_3, which feature grain boundaries. This is a rather unexpected result, however the lower electron concentration of the Ni-doped series could possibly be attributed to the fact that YSZ is an oxygen conductor, and therefore oxygen from the substrate could diffuse to the surface and deplete the SEAL. Moreover, the position of the deep acceptors in the band gap and, hence, the probability to compensate SEAL electrons, can differ.

X-ray photoelectron spectroscopy

To relate the electrical transport results to the band structure and surface band bending, XPS measurements have been performed on both the Ni-doped single-crystalline and the Mg-doped textured samples. The method probes the topmost few nanometers at the surface of the film. Figure 4 illustrates the valence band spectrum obtained by XPS for the single-crystalline UID (red) and the Ni-doped samples with $N_{\mathrm{Ni}} = 2\times10^{19}\,\mathrm{cm}^{-3}$

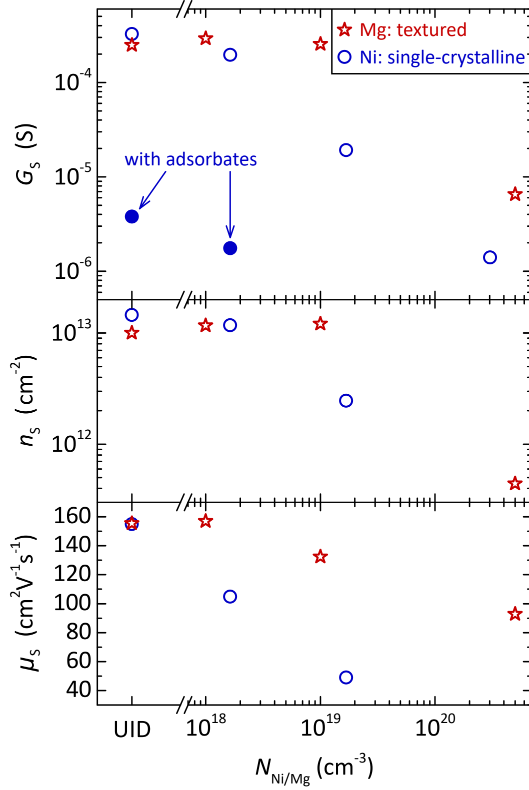

Figure 3. Transport properties of the SEAL as a function of compensating acceptor concentration $N_{\mathrm{Ni/Mg}}$: Sheet conductivity G_{S}, sheet electron concentration n_{S}, and Hall electron mobility μ_{S}. The open symbols represent the extracted data without the effect of air adsorbates (as in Eq. 3.), whereas the closed symbols correspond to the extracted SEAL transport properties with air adsorbates (Eq. 2).

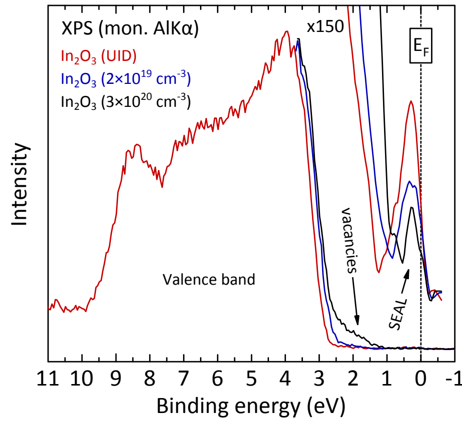

Figure 4. X-ray photoelectron spectra of the valence band and occupied conduction band states of the single-crystalline unintentionally doped (UID) and Ni-doped In_2O_3 films (Ni concentration as indicated). For the Ni-doped films, only the VB edge is shown for clarity and to depict the occurring energy shift and additional intragap states, as the shape of the complete VB spectra at higher binding energies is similar to that of the UID sample. The magnified region on the right has been smoothed (9-point locally weighted smoothing).

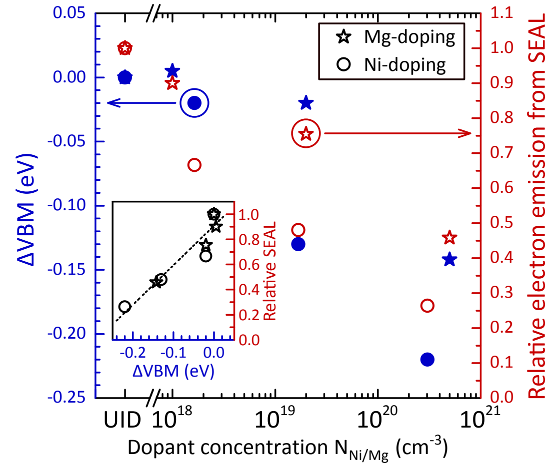

Figure 5. Change of valence band maximum ΔVBM (blue, closed points) and relative SEAL induced electron emission (red, open points) as a function of acceptor concentration $N_{\mathrm{Ni/Mg}}$ extracted from the XPS spectra. The relative electron emission values from the SEAL have been normalized with respect to the unintentionally doped reference sample. The inset shows the relative SEAL intensity (red axis) vs. ΔVBM (blue axis) including data from both In_2O_3:Ni and In_2O_3:Mg.

and $3\times10^{20}\,\mathrm{cm}^{-3}$ (blue and black respectively), after illumination with UV in vacuum, to best represent the state of the films during the transport measurements. The binding energy is presented with respect to the position of the Fermi level. The broad distribution between 10 and 3 eV originates from emission of valence band electrons[2,48,49], whereas the feature just below the E_{F} is due to partial occupation of conduction band states of the SEAL[3,9] sustained by the distinct downward bending of the electronic bands at the surface[2]. When Ni acceptors are introduced into the film, the valence band maximum (VBM) shifts towards lower binding energy for higher Ni concentrations. The same effect is observed for the core level energies. Both these shifts consistently indicate a lowering of the surface Fermi level with increasing Ni concentration. At the same time, the emission of electrons near the E_{F} from the SEAL is significantly lowered. The same effect is also observed for the Mg-doped In_2O_3 films. Furthermore, for the highest Ni concentration, an enhanced emission is observed above the VB maximum, which indicates the formation of intragap states. Such states above the VBM in In_2O_3 have been attributed to the existence of oxygen vacancies[50–52]. Their appearance at high Ni concentrations could be an indication that the incorporation of acceptors leads to a partial charge compensation by formation of additional oxygen vacancies. However, this effect has not been observed for highly Mg-doped In_2O_3 films[42].

The determination of the absolute energy of the VBM and the difference between surface E_{F} and conduction band minimum $E_{\mathrm{C_{SURF}}} - E_{\mathrm{F}}$ by XPS is not straightforward. We discuss our quantitative evaluation in the supplemental material, which results in a value of

$E_{C_{SURF}} - E_F = 0.6\,eV$ for UID In_2O_3. The change in band edge position, however, can be determined by characterizing the energy offset in XPS. We have compared the change of VBM (ΔVBM) for Ni- and Mg-doped films with varying acceptor concentrations. In addition, the area of the emission near the E_F is used as a quantitative measure of the electrons in the SEAL[33]. Both values—ΔVBM and the relative reduction of the SEAL compared to UID films—are plotted as a function of the Ni and Mg concentration in Fig. 5. It is evident that there is a correlation among the increasing acceptor concentration, the shift of VB edge towards the E_F, and the reduction of surface electron concentration. Moreover, a roughly linear relation between ΔVBM and the relative electron emission from SEAL is observed (inset of Fig. 5). In accordance with the electrical transport measurements, Ni-doping is shown to induce stronger changes in the electronic properties in comparison to the Mg-doping. Nonetheless, a significant depletion of the SEAL has been achieved, i.e. down to 26 % of that of the UID In_2O_3 for the highest Ni concentration. At this Ni concentration, however, transport measurements indicated a stronger reduction of the SEAL (conductance decrease to less than 1 % of that of the UID In_2O_3). We tentatively attribute this discrepancy to a residual O-adsorbate coverage of the adsorption-desorption equilibrium during the transport measurements under UV illumination in air.

Self-consistent Schrödinger–Poisson calculations of the near-surface potential and electron density profiles

To better understand the near-surface band and electron density profiles in the In_2O_3 films we have performed self-consistent Schrödinger–Poisson calculations varying the acceptor concentration N_A and using the experimentally determined parameters obtained from electron transport measurements and X-ray photoelectron spectroscopy as constraints. For the Poisson equation, the Dirichlet boundary conditions (i.e., fixed surface potential relative to the bulk Fermi level position) are used. We assume the full ionization of donors present in the samples, whereas for acceptors the incomplete ionization is also considered by defining the ionization energy level relative to the valence band edge. The effect of the conduction band nonparabolicity is also accounted for, and the band structure parameters as well as the dielectric parameters have been taken from Ref. 53. The net surface charge N_{SS}, corresponding to the difference $(N^+_{D,S} - N^-_{A,S})$ of the 2D concentration of charged surface donors and acceptors schematically shown in Fig. 1(c), is calculated from the charge neutrality condition applied to the entire sample.

Table I and Figure 6 summarize the major parameters and profiles based on calculations under various assumptions as described next.

Initially (Tab. I, case i) the $E_{C_{SURF}} - E_F$ from the XPS results corresponding to the UID sample, along with the

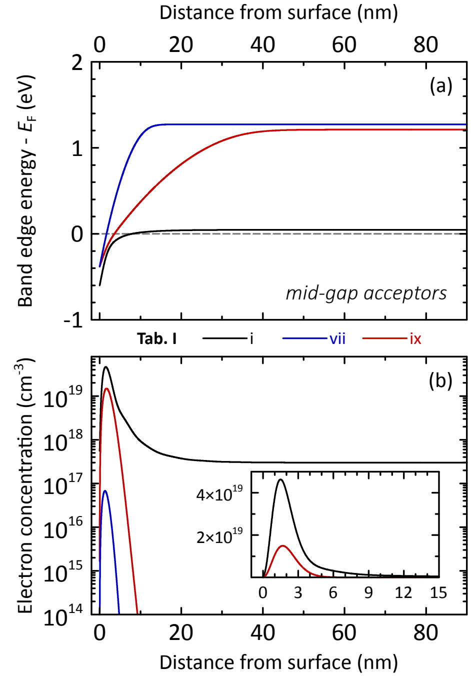

Figure 6. Band edge distributions (a) and electron concentration profiles (b) of UID (i) and acceptor-doped In_2O_3 (vii, ix) calculated by Schrödinger–Poisson calculations considering a deep acceptor level and constraints as shown in Tab. I. The inset in (b) depicts two different n_S cases in linear scale based on the experimental results from the XPS analysis of the Ni-doped films.

$E_{C_{BULK}} - E_F$ corresponding to a reasonable bulk donor concentration of $N_D = 3 \times 10^{17}\,cm^{-3}$ are used to calculate the SEAL concentration of the UID sample, n_S. The result of $n_S = 1.33 \times 10^{13}\,cm^{-2}$ matches very well the experimentally extracted results from the Hall effect measurements. N_D is assumed to correspond to singly charged donors, ignoring the possible contribution from doubly charged donors, like V_O^{2+} as previously discussed.

Next, acceptor doping is considered, where acceptors are not assumed to induce the generation of compensating donors—i.e. the donor concentration of $N_D = 3 \times 10^{17}\,cm^{-3}$ is forced to be the same as for the unintentionally doped film in case (i). If the n_S and $E_{C_{SURF}} - E_F$ from the XPS results for the sample doped with $N_{Ni} = 3 \times 10^{20}\,cm^{-3}$ are considered (0.26B) (case ii), the result would be a reduced surface states concentration, N_{ss}, and an acceptor concentration, N_A, that is significantly lower than the actual doping value. Alternatively, (case iii) fixing N_{ss} at the value (A) of the UID sample, the predicted surface Fermi energy shift of only 60 meV compared to the UID case does not match the experimental results. If the N_{ss} is kept constant at value (A) and the band edge shift from XPS are simultaneously considered (case iv), the result would correspond to complete depletion of the SEAL, even for significantly lower acceptor concentrations than the actual N_{Ni}. This result holds true irrespective of the dopant position in the band

Table I. Schrödinger–Poisson calculations for various scenarios (for detailed description see text). Values in blue have been calculated, while the rest are fixed or predefined for each case.

Nº	N_D (cm^{-3})	N_A (cm^{-3})	$N_A - N_D$ (cm^{-3})	Acceptor type	$E_{C_{BULK}} - E_F$ (eV)	$E_{C_{SURF}} - E_F$ (eV)	N_{ss} (cm^{-2})	n_S (cm^{-2})
i	3×10^{17}	—		—	0.047	-0.600	1.18×10^{13}(A)	1.33×10^{13}(B)
ii	3×10^{17}	1.0×10^{18}	7.0×10^{17}	mid-gap	1.388	-0.380	6.84×10^{12}	3.46×10^{12}(0.26B)
iii	3×10^{17}	4.3×10^{18}	4.0×10^{18}	mid-gap	1.431	-0.540	1.18×10^{13}(A)	3.46×10^{12}(0.26B)
iv	3×10^{17}	4.8×10^{18}	4.5×10^{18}	shallow	2.762	-0.380	1.18×10^{13}(A)	7.70×10^{9}
v	3×10^{17}	8.4×10^{18}	8.1×10^{18}	mid-gap	1.449	-0.380	1.18×10^{13}(A)	1.17×10^{10}
vi	2.9546×10^{20}	3.0×10^{20}	4.5×10^{18}	shallow	2.762	-0.380	1.18×10^{13}(A)	7.70×10^{9}
vii	2.9125×10^{20}	3.0×10^{20}	8.7×10^{18}	mid-gap	1.274	-0.380	1.18×10^{13}(A)	1.17×10^{10}
viii	2.9961×10^{20}	3.0×10^{20}	3.9×10^{17}	shallow	2.697	-0.380	6.80×10^{12}	3.46×10^{12}(0.26B)
ix	2.9918×10^{20}	3.0×10^{20}	8.2×10^{17}	mid-gap	1.212	-0.380	6.84×10^{12}	3.46×10^{12}(0.26B)
x	1.922×10^{19}	2.0×10^{19}	7.8×10^{17}	mid-gap	1.281	-0.380	6.84×10^{12}	3.46×10^{12}(0.26B)
xi	1.25×10^{18}	2.0×10^{18}	7.5×10^{17}	mid-gap	1.351	-0.380	6.84×10^{12}	3.46×10^{12}(0.26B)

gap, i.e. shallow (case iv) or mid-gap (case v) acceptor level of Ni. However, as both the transport measurements and the XPS results have revealed, the SEAL is still present for such low acceptor concentrations. Thus, spontaneous generation of compensating donors upon introduction of the acceptors has to be considered.

Cases (vi) and (vii) show that even if the actual acceptor concentration, N_{Ni}, and corresponding donor generation are considered, a fixed N_{ss} at the value (A) of the UID sample would predict the respective SEAL to be fully depleted, for both, shallow or mid-gap acceptor levels. Hence, the surface states concentration needs to be decreased in order to reproduce the experimental results.

Fixing the acceptor concentration at the intentional Ni-doping level of $N_{Ni} = 3 \times 10^{20}\,\mathrm{cm}^{-3}$, a comparable and, in fact, only slightly lower donor concentration (cases viii and ix) has to be considered to result in corresponding SEAL concentration $n_S = (0.26B) = 3.46 \times 10^{12}\,\mathrm{cm}^{-2}$ measured by XPS. Once again, the position of the acceptor levels in the band gap is of minimal significance to these results (viii, ix), with the N_D and N_{ss} only being slightly affected. Assuming deep acceptors—as there are indications that this is the case[54], even though they are not expected to be positioned in the middle of the band gap—and varying their concentrations by one order of magnitude at each step (cases ix-xi), we showcase that the relevant parameter for the reduction of the SEAL is $N_A - N_D$. For shallow acceptors the $N_A - N_D$ does not change at all (see supporting information).

Even though these calculations rely on certain assumptions and constraints, they allow to deduce important trends. The most important band edge and electron concentration profiles of Tab. I are plotted in Fig. 6. The inset shows the carrier distribution in a linear scale for three different n_S cases, matching the relative emission of the SEAL derived from XPS, and highlights the reduction of surface electron concentration when Ni or Mg acceptors are incorporated into the In_2O_3 layers. Integration of the profile in the inset of Fig. 6 corresponding to the acceptor-doped case (ix) indicates that the majority (approximately 90%) of the SEAL carriers are lying within 3 nm from the surface.

Consequently, no complete depletion of the In_2O_3 SEAL is achieved by acceptors at these doping concentrations, due to the spontaneous formation of compensating donors. This conclusion contrasts the findings in Mg-doped InN[23], where the lack of compensating donors results in the immense reduction of the SEAL. Nevertheless, the obtained results are promising towards the tunability of the In_2O_3 surface properties and the expansion of its potential device applications.

C. Enhanced thermopower in the SEAL 2DEG

For the determination of the Seebeck coefficient of the In_2O_3 surface, the Mg-doped sample with $N_{Mg} = 10^{19}\,\mathrm{cm}^{-3}$—with an intact SEAL and almost fully depleted parallel carrier systems—has been utilized. The effect of a weak parallel interface system has been taken into consideration and excluded using the multilayer method described previously, and specifically Eq. 5. Since the oxygen plasma treatment did not essentially affect the transport properties of this particular sample, the Seebeck coefficient was ultimately extracted from the measurements of the dark and photoreduced states of the as-grown film. The sheet electron concentration of the films has been gradually modulated using UV illumination with varying optical power between 1 and 12 mW and corresponding waiting time, which results in adsorbed, acceptorlike, oxygen species between high and low steady-state coverage. As shown in Fig. 7 (top), the Seebeck coefficient of the SEAL is negative, as expected for carrier systems with their majority carriers being electrons, and exhibits a decreasing magnitude with increasing electron concentration. Due to limitations of the external UV illumination at the Seebeck setup, it has not been possible to obtain a state of the In_2O_3 SEAL with higher electron concentration.

According to Ref. 41, the Seebeck coefficient of a two-dimensional electron gas (2DEG)—in that case ZnO—

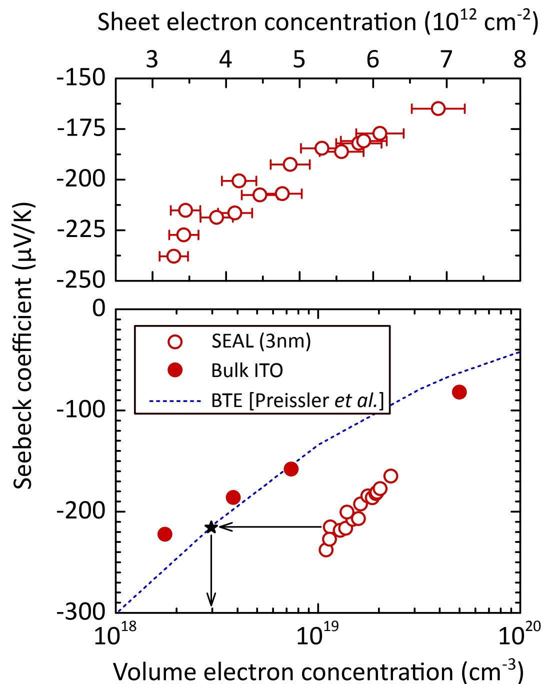

Figure 7. Top: Seebeck coefficient as a function of the surface sheet electron concentration measured by Hall effect experiments in the vdP arrangement. Bottom: comparison of the volume electron concentration of the SEAL with that of bulk ITO films and solution of the Boltzmann transport equation for $m^* = 0.3m_e$ from the work of Preissler *et al.*[45] (Fig. 9 therein).

exhibits an increased absolute value, in comparison to that of a three-dimensional electron gas (3DEG), if the semiconductor is well degenerate. This effect is also displayed in Fig. 7, where the Seebeck coefficient of the SEAL (2DEG) is compared to the experimental values of four ITO films (3DEG) as well as the theoretical curve of Ref. 45 based on the solution of the Boltzmann transport equation (BTE) for similar volume electron concentrations as that of the SEAL. This comparison yields a $\approx$ 80 % larger Seebeck coefficient of the surface 2DEG compared to a bulk 3DEG with comparable volume electron concentration. The average volume electron concentration of the SEAL has been calculated assuming that the vast majority of the carriers lie within a 3 nm thick system (cf. SP calculations of case (ix) in Tab. I and Fig. 6 for similar sheet electron concentration). That of the homogeneously Sn-doped ITO films has been obtained from Hall effect measurements and the film thickness.

Approaching it from a different perspective, if the Seebeck coefficient of the SEAL would coincide with the BTE solution of a bulk system in Fig. 7, as indicated by the black arrow for one of the data points, the corresponding average volume electron concentration of the SEAL would be significantly lower. As explained in detail in Ref. 55, the sheet and volume electron concentrations of a carrier system can be used to estimate its effective thickness, $t_{\text{eff}} = \frac{n_{2D}}{n_{3D}}$. If the volume electron concentration dictated by the BTE curve, which is valid for bulk systems, is combined with the sheet electron concentration directly measured by Hall, the resulting SEAL thicknesses would vary between 11 − 15 nm. This is a clear overestimation in comparison to both the findings of the SP calculations in Fig. 6 and previous works[9,21,56], again indicating an enhanced thermopower of the SEAL.

IV. SUMMARY AND CONCLUSION

In this work we have experimentally determined the transport properties of the In_2O_3 surface electron accumulation layer by Hall effect measurements through applying a dual-layer model in combination with plasma oxidation treatments of the surface. Oxygen adsorbates from the ambient air almost completely deplete the SEAL of an unintentionally doped film reducing its sheet conductivity to $G_S = 3.8 \times 10^{-6}$ S. Illuminating the surface with UV radiation largely removed the oxygen adsorbates, resulting in a SEAL with a sheet conductivity of $G_S = 3.26 \times 10^{-4}$ S, a sheet electron concentration of $n_S = 1.45 \times 10^{13}$ cm^{-2}, and a Hall electron mobility of $\mu_S = 155$ cm^{2}V^{-1}s^{-1}. We further demonstrated a gradual reduction of this SEAL by increasing compensating bulk acceptor doping with two different elements, namely Ni and Mg, and achieved nearly complete depletion with $N_{\text{Ni}} = 3 \times 10^{20}$ cm^{-3} doping. The gradual depletion of the SEAL with doping concentration has been confirmed by XPS measurements, able to determine the position of the valence band maximum and SEAL peak area close to the Fermi level. These results were further supported by Schrödinger–Poisson calculations, which clearly show that the introduction of acceptors in the In_2O_3 results in the subsequent generation of comparable concentrations of compensating donors. This result holds true irrespective of the position of the acceptors in the band gap, i.e. whether the corresponding levels are deep (mid-gap) or shallow. This mechanism hinders the complete depletion of the In_2O_3 SEAL. However, our results showing significant attenuation of the surface with acceptor doping are still valuable for device applications requiring tunable surface transport properties. Ultimately, the thermopower of the In_2O_3 SEAL is investigated. In agreement with previous studies on ZnO, the Seebeck coefficient of the 2DEG at the In_2O_3 surface is shown to be enhanced by $\approx$ 80 % in comparison to the 3DEG with comparable volume electron concentration in bulk ITO films.

ACKNOWLEDGMENT

We would like to thank Y. Takagaki for critically reading this manuscript, F. Gutsche for technical support with the Seebeck setup, and W. Anders for the oxygen plasma treatment of the samples. This study was

performed in the framework of GraFOx, a Leibniz ScienceCampus partially funded by the Leibniz association. We are grateful for the financial support by the Deutsche Forschungsgemeinschaft (grants BI 1754/1-1 and HI 1800/1-1).

---

[1] T. Nagata, O. Bierwagen, M. E. White, M. Y. Tsai, Y. Yamashita, H. Yoshikawa, N. Ohashi, K. Kobayashi, T. Chikyow, and J. S. Speck, Applied Physics Letters **98**, 232107 (2011).

[2] P. D. C. King, T. D. Veal, F. Fuchs, C. Y. Wang, D. J. Payne, A. Bourlange, H. Zhang, G. R. Bell, V. Cimalla, O. Ambacher, R. G. Egdell, F. Bechstedt, and C. F. McConville, Phys. Rev. B **79**, 205211 (2009).

[3] J. Rombach, A. Papadogianni, M. Mischo, V. Cimalla, L. Kirste, O. Ambacher, T. Berthold, S. Krischok, M. Himmerlich, S. Selve, and O. Bierwagen, Sens. Actuators B **236**, 909 (2016).

[4] G. S. Chae, Jpn. J. Appl. Phys. **40**, 1282 (2001).

[5] A. N. Tiwari, G. Khrypunov, F. Kurdzesau, D. L. Bätzner, A. Romeo, and H. Zogg, Prog. Photov. **12**, 33 (2004).

[6] M. Y. Tsai, O. Bierwagen, and J. S. Speck, Thin Solid Films **605**, 186 (2016).

[7] J. Michel, D. Splith, J. Rombach, A. Papadogianni, T. Berthold, S. Krischok, M. Grundmann, O. Bierwagen, H. von Wenckstern, and M. Himmerlich, ACS Applied Materials & Interfaces **11**, 27073 (2019).

[8] H. von Wenckstern, D. Splith, F. Schmidt, M. Grundmann, O. Bierwagen, and J. S. Speck, APL Materials **2**, 046104 (2014).

[9] P. D. C. King, T. D. Veal, D. J. Payne, A. Bourlange, R. G. Egdell, and C. F. McConville, Phys. Rev. Lett. **101**, 116808 (2008).

[10] A. Klein, Appl. Phys. Lett. **77**, 2009 (2000).

[11] Y. Gassenbauer, R. Schafranek, A. Klein, S. Zafeiratos, M. Hävecker, A. Knop-Gericke, and R. Schlögl, Phys. Rev. B. **73**, 245312 (2006).

[12] A. Walsh, J. L. F. D. Silva, S.-H. Wei, C. Korber, A. Klein, L. F. J. Piper, A. DeMasi, K. E. Smith, G. Panaccione, P. Torelli, D. J. Payne, A. Bourlange, and R. G. Egdell, Physical Review Letters **100**, 167402 (2008).

[13] J. Tersoff, Phys. Rev. Lett. **52**, 465 (1984).

[14] A. Schleife, F. Fuchs, C. Rödl, J. Furthmüller, and F. Bechstedt, Applied Physics Letters **94**, 012104 (2009).

[15] W. Mönch, *Semiconductor Surfaces and Interfaces* (Springer, 2001).

[16] M. Nazarzahdemoafi, F. Titze, S. Machulik, C. Janowitz, Z. Galazka, R. Manzke, and M. Mulazzi, Phys. Rev. B **93**, 081303 (2016).

[17] K. H. L. Zhang, R. G. Egdell, F. Offi, S. Iacobucci, L. Petaccia, S. Gorovikov, and P. D. C. King, Phys. Rev. Lett. **110**, 056803 (2013).

[18] A. Walsh, Applied Physics Letters **98**, 261910 (2011).

[19] M. Wagner, S. Seiler, B. Meyer, L. A. Boatner, M. Schmid, and U. Diebold, Advanced Materials Interfaces **1**, 1400289 (2014).

[20] D. W. Davies, A. Walsh, J. J. Mudd, C. F. McConville, A. Regoutz, J. M. Kahk, D. J. Payne, V. R. Dhanak, D. Hesp, K. Pussi, T.-L. Lee, R. G. Egdell, and K. H. L. Zhang, The Journal of Physical Chemistry C **123**, 1700 (2019).

[21] T. Nagata, O. Bierwagen, Z. Galazka, M. Imura, S. Ueda, Y. Yamashita, and T. Chikyow, Japanese Journal of Applied Physics **58**, SDDG06 (2019).

[22] V. Jovic, S. Moser, A. Papadogianni, R. J. Koch, A. Rossi, C. Jozwiak, A. Bostwick, E. Rotenberg, J. V. Kennedy, O. Bierwagen, and K. E. Smith, Small , 1903321 (2019).

[23] W. M. Linhart, J. Chai, R. J. H. Morris, M. G. Dowsett, C. F. McConville, S. M. Durbin, and T. D. Veal, Phys. Rev. Lett. **109**, 247605 (2012).

[24] A. Papadogianni, L. Kirste, and O. Bierwagen, Appl. Phys. Lett. **111**, 262103 (2017).

[25] O. Bierwagen and J. S. Speck, Appl. Phys. Lett. **101**, 102107 (2012).

[26] S. Lany and A. Zunger, Phys. Rev. Lett. **98**, 045501 (2007).

[27] S. Limpijumnong, P. Reunchan, A. Janotti, and C. G. Van de Walle, Phys. Rev. B **80**, 193202 (2009).

[28] P. Ágoston, K. Albe, R. M. Nieminen, and M. J. Puska, Physical Review Letters **103**, 245501 (2009).

[29] J. Buckeridge, C. R. A. Catlow, M. R. Farrow, A. J. Logsdail, D. O. Scanlon, T. W. Keal, P. Sherwood, S. M. Woodley, A. A. Sokol, and A. Walsh, Phys. Rev. Materials **2**, 054604 (2018).

[30] I. Chatratin, F. P. Sabino, P. Reunchan, S. Limpijumnong, J. B. Varley, C. G. Van de Walle, and A. Janotti, Phys. Rev. Materials **3**, 074604 (2019).

[31] G. Rupprecht, Zeitschrift für Physik **139**, 504 (1954).

[32] I.-D. Kim, A. Rothschild, and H. L. Tuller, Acta Materialia **61**, 974 (2013).

[33] T. Berthold, S. Katzer, J. Rombach, S. Krischok, O. Bierwagen, and M. Himmerlich, Physica Status Solidi B: Basic Solid State Physics **255**, 1700324 (2018).

[34] C. Xirouchaki, G. Kiriakidis, T. F. Pedersen, and H. Fritzsche, J. Appl. Phys. **79**, 9349 (1996).

[35] H. Imai, A. Tominaga, H. Hirashima, M. Toki, and N. Asakuma, J. Appl. Phys. **85**, 203 (1999).

[36] C. Y. Wang, V. Cimalla, T. Kups, C.-C. Röhlig, T. Stauden, O. Ambacher, M. Kunzer, T. Passow, W. Schirmacher, W. Pletschen, K. Köhler, and J. Wagner, Appl. Phys. Lett. **91**, 103509 (2007).

[37] C. Wang, R. Becker, T. Passow, W. Pletschen, K. Köhler, V. Cimalla, and O. Ambacher, Sensors and Actuators B: Chemical **152**, 235 (2011).

[38] H. Kind, H. Yan, B. Messer, M. Law, and P. Yang, Advanced Materials **14**, 158 (2002).

[39] O. Bierwagen, J. S. Speck, T. Nagata, T. Chikyow, Y. Yamashita, H. Yoshikawa, and K. Kobayashi, Appl. Phys. Lett. **98**, 172101 (2011).

[40] Y. Grinshpan, M. Nitzan, and Y. Goldstein, Phys. Rev. B **19**, 1098 (1979).

[41] S. Shimizu, M. S. Bahramy, T. Iizuka, S. Ono, K. Miwa, Y. Tokura, and Y. Iwasa, Proceedings of the National Academy of Sciences **113**, 6438 (2016).

[42] T. Berthold, J. Rombach, T. Stauden, V. Polyakov, V. Cimalla, S. Krischok, O. Bierwagen, and M. Himmerlich, J. Appl. Phys. **120**, 245301 (2016).

[43] K. Irmscher, M. Naumann, M. Pietsch, Z. Galazka, R. Uecker, T. Schulz, R. Schewski, M. Albrecht, and R. Fornari, physica status solidi (a) **211**, 54 (2013).
[44] M. Himmerlich, S. Krischok, V. Lebedev, O. Ambacher, and J. Schaefer, Journal of Crystal Growth **306**, 6 (2007).
[45] N. Preissler, O. Bierwagen, A. T. Ramu, and J. S. Speck, Phys. Rev. B **88**, 085305 (2013).
[46] R. Baron, G. A. Shifrin, O. J. Marsh, and J. W. Mayer, J. Appl. Phys. **40**, 3702 (1969).
[47] O. Bierwagen, S. Choi, and J. S. Speck, Phys. Rev. B **84**, 235302 (2011).
[48] P. Erhart, A. Klein, R. G. Egdell, and K. Albe, Phys. Rev. B **75**, 153205 (2007).
[49] M. Himmerlich, C. Y. Wang, V. Cimalla, O. Ambacher, and S. Krischok, Journal of Applied Physics **111**, 093704 (2012).
[50] M. Mizuno, T. Miyamoto, T. Ohnishi, and H. Hayashi, Japanese Journal of Applied Physics **36**, 3408 (1997).
[51] I. Tanaka, F. Oba, K. Tatsumi, M. Kunisu, M. Nakano, and H. Adachi, Mater. Trans. **43**, 1426 (2002).
[52] P. Ágoston, P. Erhart, A. Klein, and K. Albe, Journal of Physics: Condensed Matter **21**, 455801 (2009).
[53] M. Feneberg, J. Nixdorf, C. Lidig, R. Goldhahn, Z. Galazka, O. Bierwagen, and J. S. Speck, Phys. Rev. B **93**, 045203 (2016).
[54] H. Raebiger, S. Lany, and A. Zunger, Phys. Rev. B **79**, 165202 (2009).
[55] A. Papadogianni, M. E. White, J. S. Speck, Z. Galazka, and O. Bierwagen, Applied Physics Letters **107**, 252105 (2015).
[56] T. Nagata, O. Bierwagen, Z. Galazka, M. Imura, S. Ueda, H. Yoshikawa, Y. Yamashita, and T. Chikyow, Applied Physics Express **10**, 011102 (2017).

arXiv:2003.04631v1 [physics.app-ph] 10 Mar 2020

SUPPLEMENTAL MATERIAL
The two-dimensional electron gas of the In_2O_3 surface: Enhanced thermopower, electrical transport properties, and its reduction by adsorbates or compensating acceptor doping

Alexandra Papadogianni,[1] Julius Rombach,[1] Theresa Berthold,[2] Vladimir Polyakov,[3] Stefan Krischok,[2] Marcel Himmerlich,[2,4] and Oliver Bierwagen[1]

[1] *Paul-Drude-Institut für Festkörperelektronik, Leibniz-Institut im Forschungsverbund Berlin e.V., Hausvogteiplatz 5–7, D–10117 Berlin, Germany*

[2] *Institut für Physik und Institut für Mikro- und Nanotechnologien, Technische Universität Ilmenau, PF 100565, D–98684 Ilmenau, Germany*

[3] *Fraunhofer-Institut für Angewandte Festkörperphysik, Tullastraße 72, D-79108 Freiburg, Germany*

[4] *CERN, European Organization for Nuclear Research, 1211 Meyrin, Switzerland*

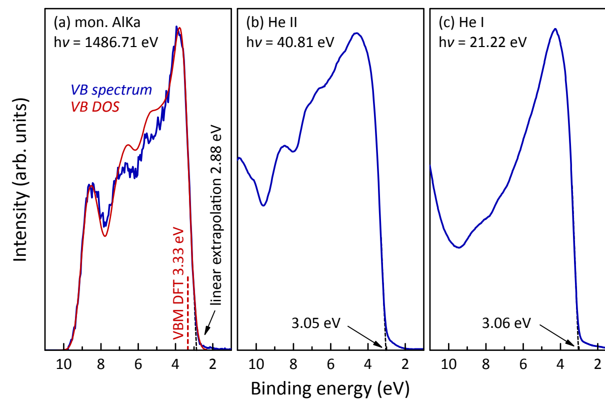

Figure 1. Comparison of the VB photoelectron spectra of a vacuum-annealed In_2O_3 reference sample excited by different light sources—from left to right: (a) AlKα, (b) He II and (c) He I radiation. The given numbers are the energy at the intersect of the linear extrapolation of the VB edge with the abscissa. The red spectrum in (a) represents the broadened VB density of states (DOS) of In_2O_3 from density-functional theory. The DOS has been shifted to match the experimental data and the corresponding VBM of the non-boradened DOS at $T = 0\,\mathrm{K}$ is 3.33 eV below the Fermi energy.

Extrapolation of the valence band edge from XPS

The determination of the absolute position of the surface valence band maximum (VBM) with respect to the Fermi energy (E_F) based on X-ray photoelectron spectroscopy (XPS) measurements is not straightforward, due to the broadening of the spectral features induced by the relative high line width (the typical Fermi edge width is approximately 300 meV). Figure (a) shows an XPS valence band spectrum of an uncontaminated In_2O_3 surface. The linear extrapolation of the VB edge gives a value of 2.88 eV, while the comparison with the broadened VB density of states[1] at $T = 0\,\mathrm{K}$ reveals a VBM position of 3.33 eV. We consider that this value would overestimate the actual VBM, since a thermal broadening as well as uncertainties in DFT calculations have to be considered. Comparing the corresponding ultraviolet photoelectron spectroscopy (UPS) VB spectra with higher surface sensitivity, we obtain a VBM of approximately 3.1 eV below the E_F. In this case, the experimental resolution is in the range of 50 meV, which is considerably low to allow for reliable estimations. Considering the band gap range of In_2O_3 (2.6–2.8 eV) and the possible band gap renormalization, due to conduction band occupation below 100 eV, in the case where the electron concentration stays in the $10^{19}\,\mathrm{cm}^{-3}$ range[2], we estimate the position of the conduction band minimum for the UID In_2O_3 to be 0.6 eV below the E_F.

For samples that have been exposed to air after growth, UPS measurements are not applicable to determine the VBM, since the spectral features mainly include features of the surface adsorbates. We did not intend to use thermal vacuum treatments to clean the surface of the Ni- and Mg-doped films from adsorbates, which could potentially induce modifications of the electronic properties, doping characteristics and possibly induce other types of defects (mainly creation of donors due to oxygen vacancy formation). Consequently, such UPS measurements could not be implemented in this case. However, having defined a reference value for the XPS VB spectrum of clean UID In_2O_3 as described above, we can rely on the VB shifts determined by extrapolation of the XPS spectra, since changes in band bending affect the binding energy scale directly. It is often argued that XPS averages over a certain depth range and hence does not directly allow to determine VB shifts correctly. It needs to be pointed out that the main signal still originates directly from the topmost few nanometers of the surface and a linear extrapolation determines the upper edge of the VB depth profile, even though the high binding energy side might be broadened or narrowed. The trends of band edge shifts are anyways reflected correctly and there might only exists a slight underestimation of ΔVBM for the presented measurements.

Detailed Schrödinger–Poisson calculations and the case of shallow acceptors

Tables I and II show the full list of Schrödinger–Poisson (SP) calculations performed to get a deeper understanding of the band alignment and transport properties of the SEAL in acceptor-doped In_2O_3 for the case of deep (mid-gap)–extensively discussed in the main manuscript—and shallow acceptor levels respectively. These tables also include the cases discussed in detail in the main manuscript. Figure 2 presents the depth profiles of the band edge energy relative to the Fermi level E_F and electron concentration for mid-gap (left, exactly as presented in the manuscript) and shallow (right) acceptors. The profiles describe the UID (i) and acceptor-doped cases matching the n_S observed

Table I. Schrödinger–Poisson calculations for various scenarios assuming deep (mid-gap) acceptor levels lying close to the middle of the band gap. Values in blue have been calculated, while the rest are fixed or predefined for each case.

Case	N_D (cm^{-3})	N_A (cm^{-3})	$N_A - N_D$ (cm^{-3})	$E_{C_{BULK}} - E_F$ (eV)	$E_{C_{SURF}} - E_F$ (eV)	N_{ss} (cm^{-2})	n_S (cm^{-2})
i	3×10^{17}	—		0.047	-0.600	1.18×10^{13}(A)	1.33×10^{13}(B)
ii	3×10^{17}	6.7×10^{17}	3.7×10^{17}	1.370	-0.470	8.75×10^{12}	6.38×10^{12}(0.48B)
iii	3×10^{17}	1.0×10^{18}	7.0×10^{17}	1.388	-0.380	6.84×10^{12}	3.46×10^{12}(0.26B)
iv	1.25×10^{18}	2.0×10^{18}	7.5×10^{17}	1.351	-0.380	6.84×10^{12}	3.46×10^{12}(0.26B)
v	1.921×10^{19}	2.0×10^{19}	7.9×10^{17}	1.281	-0.380	6.84×10^{12}	3.46×10^{12}(0.26B)
vi	1.9918×10^{20}	2.0×10^{20}	8.2×10^{17}	1.222	-0.380	6.84×10^{12}	3.46×10^{12}(0.26B)
vii	2.9918×10^{20}	3.0×10^{20}	8.2×10^{17}	1.212	-0.380	6.84×10^{12}	3.46×10^{12}(0.26B)
viii	3×10^{17}	4.3×10^{18}	4.0×10^{18}	1.431	-0.540	1.18×10^{13}(A)	3.46×10^{12}(0.26B)
ix	3×10^{17}	8.4×10^{18}	8.1×10^{18}	1.449	-0.380	1.18×10^{13}(A)	1.17×10^{10}
x	1.1692×10^{19}	2.0×10^{19}	8.3×10^{18}	1.355	-0.380	1.18×10^{13}(A)	1.17×10^{10}
xi	1.9132×10^{20}	2.0×10^{20}	8.7×10^{18}	1.284	-0.380	1.18×10^{13}(A)	1.17×10^{10}
xii	2.9125×10^{20}	3.0×10^{20}	8.8×10^{18}	1.274	-0.380	1.18×10^{13}(A)	1.17×10^{10}

Table II. Schrödinger–Poisson calculations for various scenarios assuming shallow acceptor levels lying close to the valence band edge. Values in blue have been calculated, while the rest are fixed or predefined for each case.

Case	N_D (cm^{-3})	N_A (cm^{-3})	$N_A - N_D$ (cm^{-3})	$E_{C_{BULK}} - E_F$ (eV)	$E_{C_{SURF}} - E_F$ (eV)	N_{ss} (cm^{-2})	n_S (cm^{-2})
i	3×10^{17}	—		0.047	-0.600	1.18×10^{13}(A)	1.33×10^{13}(B)
ii	3×10^{17}	5.0×10^{17}	2.0×10^{17}	2.679	-0.470	8.73×10^{12}	6.38×10^{12}(0.48B)
iii	3×10^{17}	6.9×10^{17}	3.9×10^{17}	2.697	-0.380	6.80×10^{12}	3.46×10^{12}(0.26B)
iv	1.61×10^{18}	2.0×10^{18}	3.9×10^{17}	2.697	-0.380	6.80×10^{12}	3.46×10^{12}(0.26B)
v	1.961×10^{19}	2.0×10^{19}	3.9×10^{17}	2.697	-0.380	6.80×10^{12}	3.46×10^{12}(0.26B)
vi	1.9961×10^{20}	2.0×10^{20}	3.9×10^{17}	2.697	-0.380	6.80×10^{12}	3.46×10^{12}(0.26B)
vii	2.9961×10^{20}	3.0×10^{20}	3.9×10^{17}	2.697	-0.380	6.80×10^{12}	3.46×10^{12}(0.26B)
viii	3×10^{17}	2.6×10^{18}	2.3×10^{18}	2.743	-0.540	1.18×10^{13}(A)	3.46×10^{12}(0.26B)
ix	3×10^{17}	4.8×10^{18}	4.5×10^{18}	2.762	-0.380	1.18×10^{13}(A)	7.70×10^{9}
x	1.546×10^{19}	2.0×10^{19}	4.5×10^{18}	2.762	-0.380	1.18×10^{13}(A)	7.70×10^{9}
xi	1.9546×10^{20}	2.0×10^{20}	4.5×10^{18}	2.762	-0.380	1.18×10^{13}(A)	7.70×10^{9}
xii	2.9546×10^{20}	3.0×10^{20}	4.5×10^{18}	2.762	-0.380	1.18×10^{13}(A)	7.70×10^{9}

by XPS for the Ni-doped sample with $N_{Ni} = 3 \times 10^{20}\,\mathrm{cm}^{-3}$ (vii) and assuming that the concentration of surface states remains unchanged (xii), which proves to incorrectly represent the real experimental results, as it leads to a depleted SEAL. Comparing the deep and shallow acceptor cases one can conclude that the position of the acceptor level in the band gap does not significantly affect the SEAL. The parameter $N_A - N_D$ is the most relevant to obtain a certain value for n_S, if a fixed value for $E_{C_{SURF}} - E_F$ is taken into consideration. This becomes particularly apparent for the shallow acceptor case, where the $N_A - N_D$ remains constant: see Tab. II realistic cases (iii-vii) describing a $n_S = 3.46 \times 10^{12}\,\mathrm{cm}^{-2}$ and cases (ix-xii) assuming an unchanged N_{ss} and depleted SEAL.

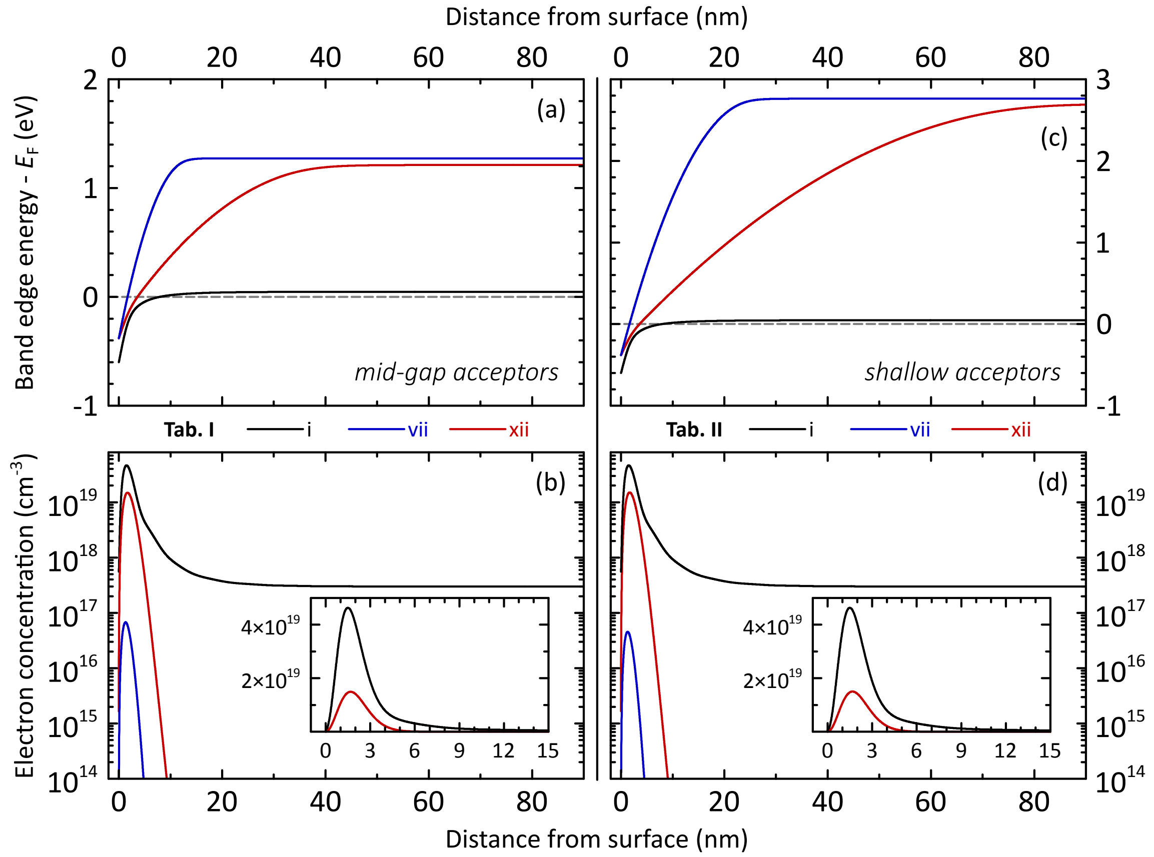

Figure 2. Band edge distributions (a, c) and electron concentration profiles (b, d) of UID (i) and acceptor-doped In_2O_3 (vii, xii) calculated by Schrödinger–Poisson calculations considering either deep (a, b) or shallow acceptor levels (c, d) and constraints as shown in Tab. I and Tab. II respectively. The insets depict different n_S cases in linear scale based on the experimental results from the XPS analysis of the Ni-doped films.

[1] P. D. C. King, T. D. Veal, F. Fuchs, C. Y. Wang, D. J. Payne, A. Bourlange, H. Zhang, G. R. Bell, V. Cimalla, O. Ambacher, R. G. Egdell, F. Bechstedt, and C. F. McConville, Phys. Rev. B **79**, 205211 (2009).
[2] M. Feneberg, J. Nixdorf, C. Lidig, R. Goldhahn, Z. Galazka, O. Bierwagen, and J. S. Speck, Phys. Rev. B **93**, 045203 (2016).